CONCEPTS IN SURFACE ALLOYING OF METALS

Santosh S. Hosmani[*]

Department of Metallurgy and Materials Science, College of Engineering, Pune (COEP), Shivaji Nagar, Pune - 411005, Maharashtra, India

Abstract

Surface alloying is widely used method in industries to improve the surface properties of metals/alloys. Significance of the various surface engineering techniques to improve the properties of engineering components in various applications, for example, automobile industries, has grown substantially over the many years. The current paper is focused on the fundamental scientific aspects of the surface alloying of metals. Widely used surface alloying elements involved are interstitial elements such as nitrogen, carbon, and substitutional element, chromium. This topic is interdisciplinary in nature and various science and engineering streams can work together for the further development in this topic. This paper has attempted to cover the essential concepts of surface alloying along with some of the interesting results in this research area.
Keywords: nitriding, carburizing, chromizing, hardness

General introduction

In many engineering applications, surface properties have a significant impact on the life of the metallic components because the functions need to be performed by the surface are different than the functions to be performed by the bulk of the components. There are many methods for surface alloying of ferrous alloy components by using techniques like, pack, gaseous, plasma, ion beam, and salt-bath. Using the effective surface treatment, less expensive grades of alloys can possibly be used for comparable or even improved service life and performance. Carburizing and nitriding are well-known thermochemical surface treatments to improve the fatigue, tribological and/or anti-corrosion properties of steel components. There are several surface hardening methods available. One method is, to introduce carbon or nitrogen in a specimen. If strong carbide/nitrides forming alloying elements like Ti, Al, V, Cr, Mo and/or W are finely dispersed in the matrix, they form carbide/nitride precipitates, which cause large

---

[*] Corresponding Author: Santosh S. Hosmani, santosh.hosa@gmail.com

increase in the hardness. Hard surface layer and ductile core improve also improves the load bearing capability of the component, for example, austenitic stainless steel.

Upon carburising, carbon is incorporated into the surface region of an iron based alloys at usually much high treatment temperatures in the range of 900 – 1050 °C (within austenitic regime). In contrast, nitriding is performed at temperatures in the range of 450 – 590 °C, i.e. below the binary eutectoid temperatures (within ferritic regime) of the Fe–N solid solution [1]. Compared to carburizing, negligible changes of the dimensions of the specimens occur upon nitriding, since the bulk remains ferritic during the treatment.

Nitrided regions can be subdivided into: (i) the compound layer adjacent to the surface composed of iron nitrides, and (ii) the diffusion zone underneath, where nitrogen is either dissolved or precipitated as nitrides (Figure 1). The improvement of corrosion and wear properties can be attributed to the compound layer, whereas the diffusion zone improves the fatigue properties, if precipitation of nitrides takes place.

There are several nitriding methods: e.g. plasma nitriding, salt bath nitriding and gaseous nitriding. The most well-known method to introduce nitrogen into a (ferritic) specimen is gaseous nitriding. An eminent advantage of gaseous nitriding is the precise control of the chemical potential of nitrogen in the nitriding atmosphere. At the constant nitriding temperature, by controlling the chemical potential of nitrogen in the atmosphere, it is possible to avoid the formation of compound layer.
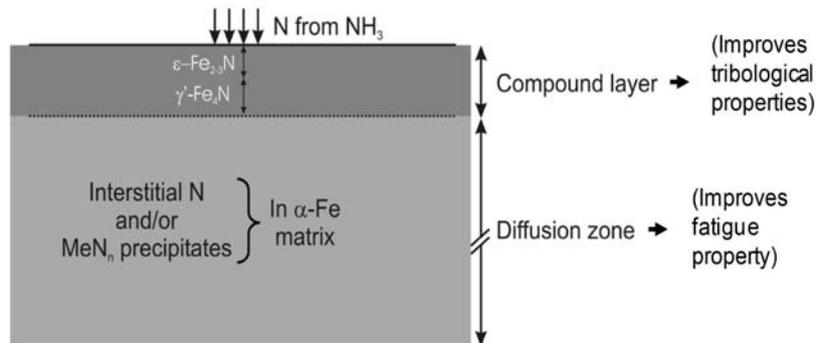
Figure 1. Schematic presentation of the surface region of a nitrided iron/iron-based alloy.

Since carburizing is done at high temperature, i.e. within the austenite phase region, the chance of the formation of cementite (Fe_3C) layer is poor. But, if the chemical potential of carbon in the carburizing atmosphere is very high, cementite formation at the surface can occur. Due to the high temperature, dissociation of such cementite leads to the *metal-dusting* problem: $Fe_3C \rightarrow 3\ Fe_{dust} + C_{graphite}$. At low temperature (i.e. below about 800 °C), pack-carburizing will not be successful due to the inability of solid pack-mixture to generate enough CO gas in the pack. In case of the gas-carburizing, using the controlled atmosphere of CO, CO_2 and N_2 gas mixture, successful carburizing is possible even at lower temperature. The surface region of the carburized iron-based alloy appears similar to that of nitrided alloy. However, the difference is the possibility of formation of cementite layer as a compound layer and the diffusion zone consists of carbides plus dissolved carbon in the surrounding matrix.

Similar to the carburizing and nitriding, chromizing is one of the widely used surface alloying technologies to improve the high temperature oxidation and corrosion resistance of specimens economically. Various chromizing processes have been developed, for example, pack cementation method, molten-salt technique and vacuum chromizing process. Pack-cementation is one of the cheapest processes (in comparison with other methods, such as CVD, plasma, vacuume based etc methods) for chromizing. Due to the larger size of the chromium atom than carbon/nitrogen atom, the diffusion of chromium is lower than the diffusion of carbon in steel at any given temperature of the solid phase. Therefore, the chromizing is done at temperatures above 1000 °C.

Mechanism of surface alloying

The mechanism of surface alloying generally involves *three* steps, which are as follows:

- *Absorption of diffusing species at specimen surface*: Driving force for this absorption is the difference in chemical potential (or activity) of diffusing species in the surrounding atmosphere ($\mu_{\text{surrounding}}$) and at the surface of specimen (μ_{surface}). At initial stage, absorption of the diffusing species at the surface is high because the difference between $\mu_{\text{surrounding}}$ and μ_{surface} is high. Maximum surface concentration of the species depends upon $\mu_{\text{surrounding}}$. The absorption of species at the surface generates its concentration gradient.
- *Inward diffusion of the absorbed species*: This causes the transport of species to deeper depths in the cross-section.
- *Formation of compounds*: This depends upon the interaction of diffusing species with elements present in the specimen.

Carburizing and nitriding potential

The ability of carburizing/nitriding atmosphere to introduce carbon/nitrogen into the surface of specimen depends upon the chemical potential of carbon/nitrogen in the atmosphere. The carbon transfer from CO to the solid can occur in principle via the following reactions:

$$2CO \Leftrightarrow [C] + CO_2 \tag{1}$$

$$CO + H_2 \Leftrightarrow [C] + H_2O \tag{2}$$

where [C] denotes carbon dissolved in the iron matrix or in a carbide. It has been shown experimentally that the heterogeneous water-gas reaction (Eq. (2)) is considerably faster than the Boudouard reaction (Eq. (1)) [2]. The necessary H_2 for undergoing Eq. (2) is either provided directly or as a result of the thermal dissociation of NH_3 (in case of nitrocarburising).

If local equilibrium between the gas phase and the solid exists, it follows that the carbon activity, a_C, obeys [3, 4]:

$$a_C^S = K^{(1)} r_C^{(1)} \tag{3}$$

$$a_C^S = K^{(2)} r_C^{(2)} \tag{4}$$

where $K^{(1)}$ and $K^{(2)}$ are the equilibrium constants for Eqs. (1) and (2) respectively, and $r_C^{(1)}$ and $r_C^{(2)}$ are the corresponding "carburising potentials":

$$r_C^{(1)} = \frac{p_{CO}^2}{p_{CO_2}} \tag{5}$$

$$r_C^{(2)} = \frac{p_{CO} \cdot p_{H_2}}{p_{H_2O}} \tag{6}$$

where p_{CO}, p_{CO2}, p_{H_2} and p_{H_2O} are the partial pressures of CO, CO$_2$, H$_2$ and H$_2$O gases, respectively.

The "nitriding potential", r_N, is defined as follows,

$$r_N = \frac{p_{NH_3}}{p_{H_2}^{3/2}} \tag{7}$$

where, p_{NH_3} and p_{H_2} are the partial pressures of NH$_3$ and H$_2$, respectively. Nitriding in a NH$_3$-H$_2$ gas mixture can be presented as [3]:

$$NH_3 \Leftrightarrow [N] + \frac{3}{2} H_2 \tag{8}$$
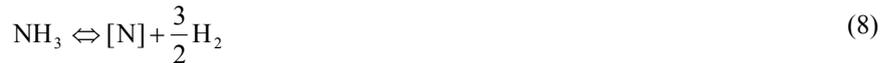
where [N] represents nitrogen dissolved in the ferrite grains of the iron-chromium alloy. Thus, if local equilibrium occurs at the surface of the specimen, the activity of nitrogen in the specimen at its surface, a_N^S, and the chemical potential of nitrogen in the gas phase are both governed by r_N, irrespective of the total pressure of the NH$_3$-H$_2$ gas mixture. Thus, it holds for a_N^S:

$$a_N^S = K^{(8)} \left(\frac{p_{NH_3}}{p_{H_2}^{3/2}} \right) = K^{(8)} r_N \tag{9}$$

where $K^{(8)}$ is the equilibrium constant for reaction (8). Hence, by controlled variation of the gas composition in the nitriding atmosphere, the activity of nitrogen at

the surface and thereby the concentration of dissolved nitrogen at the surface can be varied [4].

Equilibrium of nitriding atmosphere with iron surface

Gaseous nitriding in controlled atmosphere is close to equilibrium system compared with plasma processes. Therefore, gaseous nitriding is considered here.

Nitriding in NH_3-H_2 gas mixture is equivalent to nitriding in N_2 at a pressure of a number of thousands atm (thermodynamic argument [3]) and is possible due to the slow thermal decomposition of NH_3 (kinetic argument [4]). Therefore the Fe-N phase diagram established in contact with NH_3-H_2 gas mixture is not the phase diagram for its pure components Fe and N_2 at atmospheric pressure, but, it represents the phase diagram for Fe and NH_3-H_2 gas mixture.

The chemical potential of nitrogen in a gas phase, $\mu_{N,g}$, consisting of an NH_3-H_2 gas mixture can be defined on the basis of the hypothetical equilibrium:
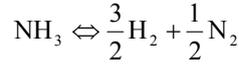
$$NH_3 \Leftrightarrow \frac{3}{2}H_2 + \frac{1}{2}N_2$$

where,

$$\mu_{N,g} \equiv \frac{1}{2}\mu_{N_2} = \mu_{NH_3} - \frac{3}{2}\mu_{H_2}$$

If the standard states refer to unit pressure and if ideal gases or constant fugacity coefficients can be assumed it holds:

$$\mu_{N,g} = \frac{1}{2}\left[G_{N_2}^0 + RT \ln p_{N_2}\right] = \left[\left(G_{NH_3}^0 + RT \ln p_{NH_3}\right) - \left(\frac{3}{2}G_{H_2}^0 + RT \ln p_{H_2}^{3/2}\right)\right]$$

$$= G_{NH_3}^0 - \frac{3}{2}G_{H_2}^0 + RT \ln\left(\frac{p_{NH_3}}{p_{H_2}^{3/2}}\right)$$

$$= G_{NH_3}^0 - \frac{3}{2}G_{H_2}^0 + RT \ln(r_n) \tag{10}$$

where p_{N_2}, p_{HN_3} and p_{H_2} are partial pressure of N_2, NH_3 and H_2 respectively; G is Gibbs-free energy per mole and superscript 0 indicates the standard state; r_n is nitriding potential. From Eq. (1.10), at constant temperature $\mu_{N,g}$ depends only on r_n. If equilibrium is attained between an imposed NH_3-H_2 gas mixture and Fe-N phase (i.e. in present study "say" α-Fe), the chemical potential of nitrogen in α-Fe is equal to that in the gas phase: $\mu_{N,\alpha-Fe} = \mu_{N,g}$. By variation of the NH_3/H_2 gas mixture (i.e. variation nitriding potential) at a certain temperature and determination of the equilibrium nitrogen content in the α-Fe phase the so-called nitrogen absorption isotherm for Fe in α-phase region can be determined.

A solution of nitrogen in ferrite can be described considering a regular solution of nitrogen on its own sublattice [5]. The nitrogen content on the interstitial sublattice is so low that excess enthalpy does not need to be taken into account [5]. So now the Gibbs-free energy for one mole Fe-N (α phase) reads [6]:

$$
\begin{aligned}
G_{Fe-y_{N,\alpha}} = &G_{Fe}^0 + y_{N,\alpha-Fe} \cdot G_{N,\alpha-Fe}^0 + \\
&+ RT\big[y_{N,\alpha-Fe} \cdot \ln(y_{N,\alpha-Fe}) + (1-y_{N,\alpha-Fe}) \cdot \ln(1-y_{N,\alpha-Fe})\big]
\end{aligned}
\tag{11}
$$

where $y_{N,\alpha-Fe}$ is the fraction of sites of 'interstitial sublattice' that is occupied by N atoms (i.e. occupancy of nitrogen sublattice for α-Fe phase). A general representation of the chemical potential [4] of nitrogen in ferrite:

$$
\mu_{N,\alpha-Fe} \equiv N_{Av}\left(\frac{\partial G_{Fe-y_{N,\alpha}}^|}{\partial y_{N,\alpha-Fe}}\right) = \left(\frac{\partial G_{Fe-y_{N,\alpha}}}{\partial y_{N,\alpha-Fe}}\right)
\tag{12}
$$

where the symbol $G^|$ refers to the Gibbs-free energy of the whole system; and symbol G denotes to the molar free energy which is independent of the size of the system. N_{Av} is Avogadro's number.

Now, from Eqs. (11) and (12), the chemical potential of nitrogen in ferrite, $\mu_{N,\alpha-Fe}$, is:

$$
\mu_{N,\alpha-Fe} = G_{N,\alpha-Fe}^0 + RT\ln\left[\frac{y_{N,\alpha-Fe}}{1-y_{N,\alpha-Fe}}\right]
\tag{13}
$$

For equilibrium between NH_3-H_2 gas mixture and ferrite: $\mu_{N,\alpha-Fe} = \mu_{N,g}$, equating Eq. (10) and (13):

$$
G_{N,\alpha-Fe}^0 + RT\ln\left[\frac{y_{N,\alpha-Fe}}{1-y_{N,\alpha-Fe}}\right] = G_{NH_3}^0 - \frac{3}{2}G_{H_2}^0 + RT\ln(r_n)
$$

i.e.
$$
G_{N,\alpha-Fe}^0 - G_{NH_3}^0 + \frac{3}{2}G_{H_2}^0 = RT\ln(r_n) - RT\ln\left[\frac{y_{N,\alpha-Fe}}{1-y_{N,\alpha-Fe}}\right]
\tag{14}
$$

Let, ΔG^0 be the change in standard Gibbs-free energy for the solubility of nitrogen in ferrite in equilibrium with NH_3-H_2 gas mixture:

$$
NH_3 - \frac{3}{2}H_2 \Leftrightarrow [N]_\alpha
\tag{15}
$$

For the above reaction (Eq. (15)) ΔG^0 is,

$$\Delta G^0 = G^0_{N,\alpha-Fe} - G^0_{NH_3} + \frac{3}{2}G^0_{H_2} = -RT\ln\left(\frac{a^0_n}{p^0_{NH_3} \cdot (p^0_{H_2})^{-3/2}}\right) \qquad (16a)$$

In the standard state, activity of dissolved N in ferrite, $a^0_n = 1$ and let $[p^0_{NH_3} \cdot (p^0_{H_2})^{-3/2}]$ be r^0_n (where r^0_n is reference nitriding potential for α-Fe phase). So Eq. (16a) becomes,

$$\Delta G^0 = G^0_{N,\alpha-Fe} - G^0_{NH_3} + \frac{3}{2}G^0_{H_2} = RT\ln(r^0_n) \qquad (16b)$$

From Eqs. (14) and (16b),

$$RT\ln(r^0_n) = RT\ln(r_n) - RT\ln\left[\frac{y_{N,\alpha-Fe}}{1-y_{N,\alpha-Fe}}\right]$$

i.e. $\left[\dfrac{y_{N,\alpha-Fe}}{1-y_{N,\alpha-Fe}}\right] = \left[\dfrac{r_n}{r^0_n}\right]$ \qquad (17)

Since the occupancy of nitrogen for α-Fe phase ($y_{N,\alpha-Fe}$) is very small, the denominator in left-hand-side of Eq. (17) can be replaced by 1:

$$y_{N,\alpha-Fe} = \frac{r_n}{r^0_n} \qquad (18)$$

According to Eq. (18) the equilibrium nitrogen content in α-Fe at a certain temperature depends linearly on the nitriding potential. Such simple straightforward relations do not occur for other Fe-N phases, like $\gamma^|$-Fe_4N_{1-x} and ϵ-Fe_2N_{1-z} (see Refs. [4, 5] for details).

Putting, $\Delta G^0 = \Delta H^0 - T\Delta S^0$ in Eq. (16b) gives,

$$RT\ln(r^0_n) = \Delta H^0 - T\Delta S^0 \qquad (19a)$$

i.e. $\ln(r^0_n) = \left(\dfrac{-\Delta S^0}{R}\right) + \left(\dfrac{\Delta H^0}{R}\right)\dfrac{1}{T}$ \qquad (19b)

From Eqs. (18) and (19b),

$$\ln(r^0_n) = -\ln\left(\frac{y_{N,\alpha-Fe}}{r_n}\right) = \left(\frac{-\Delta S^0}{R}\right) + \left(\frac{\Delta H^0}{R}\right)\frac{1}{T} \qquad (20c)$$

The solubility of nitrogen in ferrite within the temperature range of 300-600 °C is given by:

$$\log\left(\frac{y_{N,\alpha-Fe}}{r_n}\right) = 7.589 - \frac{4025}{T} \quad \text{(Ref. [7])} \tag{21}$$

$$\log\left(\frac{y_{N,\alpha-Fe}}{r_n}\right) = 7.395 - \frac{3880}{T} \quad \text{(Ref. [8])} \tag{22}$$

where T, $y_{N,\alpha-Fe}$ and r_n are in K, at.% and Pa$^{-1/2}$ respectively.

Diffusion and case depth

Thickness of surface alloyed layer is an important criterion in designing the components in various applications. Layer thickness depends on the rate of transfer of species, i.e. diffusion phenomena.

Diffusion occurs to produce decrease in Gibbs free energy. In practice, it is usually assumed that diffusion occurs down the concentration gradients ("down-hill" diffusion). However, this is true under special situations and there are some occasions where diffusion can occur up the concentration gradient ("up-hill" diffusion). Therefore, the most appropriate explanation for the driving force for diffusion is "chemical potential gradient". As a simple illustration of this consider Figure 2. Two alloys of A-B solid solution, with different compositions (alloy-1 contains X_1 atom fraction of B and the alloy-2 contains X_2 atom fraction of B), are welded together and held at a high temperature. Change in the molar free energy with composition is shown in Fig. 2. G_1 and G_2 are the molar free energies of alloys 1 and 2 respectively. Tangents drawn to the free energy curve at X_1 and X_2 give the chemical potentials (μ) of A and B in both alloys. Chemical potential of A is higher in the alloy-1, whereas the chemical potential of B is higher in the alloy-2. Therefore, A atoms diffuse from alloy-1 to 2 and B atoms diffuse from alloy-2 to 1. Such diffusion continues till the molar free energy of both alloys decreases to G_3.
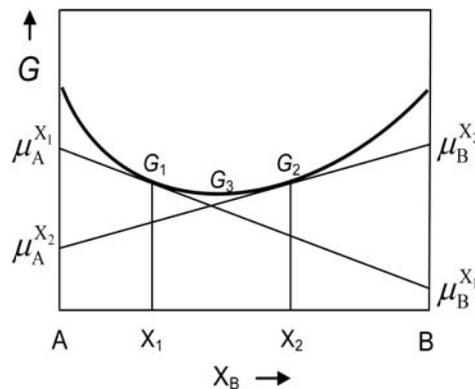
Figure 2. Free energy and chemical potential changes during diffusion.

There are two widely known mechanisms by which atoms can diffuse through the specimen: (i) substitutional diffusion (which requires the presence of vacancies), and (ii) interstitial diffusion. Activation energy barrier for substitutional diffusion is larger than the interstitial diffusion. This is because substitutional atoms are larger in size compared with interstitial atoms (e.g. carbon and nitrogen) and, also, substitutional diffusion requires creation of vacancies.

The diffusion coefficient, D, increases with temperature. The usual temperature dependence for the diffusion coefficient (D) reads:

$$D = D_0 \cdot \exp\left(\frac{-Q}{RT}\right) \tag{23}$$

where D_0 is pre-exponential factor; Q is the activation energy for diffusion and R is the universal gas constant (= 8.314 J mol^{-1} K^{-1}). An Arrhenius plot gives the linear dependence of logarithm of D with inverse of T, where slope of the line gives Q and intercept on Y-axis gives D_0.

Diffusion coefficient (diffusivity) of carbon in ferrite (α-Fe) and austenite (γ-Fe) is given by the following expressions [9]:

$$D_C^{\alpha-Fe} = (6.2 \times 10^{-7}) \cdot \exp\left(\frac{-80000}{RT}\right) \text{ m}^2 \text{ sec}^{-1} \tag{24}$$

$$D_C^{\gamma-Fe} = (2.3 \times 10^{-5}) \cdot \exp\left(\frac{-148000}{RT}\right) \text{ m}^2 \text{ sec}^{-1} \tag{25}$$

At a given temperature, diffusion of carbon in austenite (face centered cubic, f.c.c., iron) is more difficult than in ferrite (body centered cubic, b.c.c., iron), as indicated by the higher activation energy barrier for diffusion of carbon in γ-Fe than in α-Fe, because f.c.c. crystal structure closely packed than b.c.c. structure (atomic packing efficient of 74% for f.c.c. versus 68% for b.c.c.).

Diffusion coefficient of nitrogen in ferrite is given by the following expressions [10]:

$$D_N^{\alpha-Fe} = (6.6 \times 10^{-7}) \cdot \exp\left(\frac{-77822}{RT}\right) \text{ m}^2 \text{ sec}^{-1} \tag{26}$$

From Eqs. (24) and (26), the diffusivity of nitrogen in ferrite is slightly easier than that of carbon.

There are two types of diffusion processes: (i) steady-state diffusion, and (ii) non-steady state diffusion.

i. *Steady-state diffusion*: in this case, concentration gradient is constant and diffusing flux does not change with time, for example, diffusion of a gas through a plate of metal (of thickness *d*) for which pressure (or concentration) of gas is held constant (C_1 and C_2) on both sides of the plate (Figure 3). For the constant values of C_1 and C_2, if thickness of the plate is increased, diffusing flux will decrease.
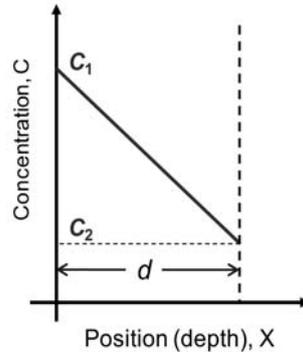
Figure 3. Fick's first law demonstrated by the diffusion of a gas through a plate of metal with thickness d.

Flux of the diffusing species is given by Fick's first law:

$$J = -D\frac{dC}{dX} \qquad (27)$$

Flux, *J*, is a measurement of the number of atoms per unit area that cross a particular plane per unit time. *D* is the diffusivity of the diffusing species.

ii. *Non-steady state diffusion*: most practical diffusion situations are non-steady state (e.g. nitriding, carburizing), i.e. concentration gradient, dC/dX, is a function of time, *t* (see Figure 4). Change in the concentration with depth and time is give by Fick's second law:

$$\frac{dC}{dt} = D\frac{\partial^2 C}{\partial X^2} \qquad (28)$$

In Eq. (28), *D* is assumed to be independent of concentration. The solution to Eq. (28) for unidirectional diffusion from one medium to another across a common interface is of the general form:

$$C(X,t) = A - B\,erf\left(\frac{X}{2\sqrt{Dt}}\right) \qquad (29)$$

where *A* and *B* are constants to be determined from the initial and boundary conditions of a particular problem. Here, the diffusion direction X is perpendicular to the common interface between the surface-alloying atmosphere and specimen surface. The origin for X is at the interface. The two media are taken to be semi-infinite, i.e. only one end of each of them (which is at the interface) is defined. The other two ends are at an infinite distance. The solution of Eq. (28) for carburizing of steel can be obtained by considering the following bounder conditions (see also Figure 4),

For t = 0, C = C_0 at x > 0
For t > 0, C = C_s at x = 0
C = C_0 at x = ∞
which gives,

$$C(X,t) = C_s - (C_s - C_0)\,erf\left(\frac{X}{2\sqrt{Dt}}\right) \qquad (30)$$
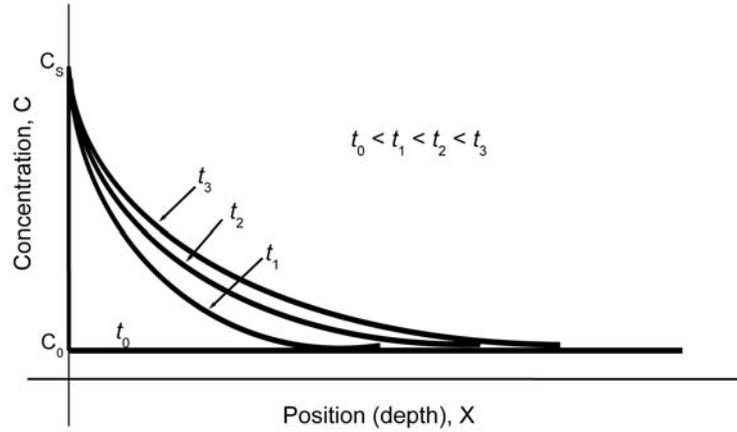
Figure 4. Fick's second law demonstrated by the change in concentration-depth profile with time.

The first proposals to describe diffusion zone growth upon nitriding are based on a simple model originally meant for "internal oxidation" [11]. This model can be applied to internal nitriding by considering the following assumptions [12]:

i. The nitrogen dissolved in the ferrite matrix (α) exhibits Henrian behaviour. This implies that the diffusion coefficient of nitrogen in the ferrite matrix is independent of the dissolved nitrogen content.

ii. The reaction of dissolved nitrogen with dissolved nitride forming alloying element (Me), leading to the nitride MeN_n, takes place only and completely at a sharp interface between the nitrided zone and the non-nitrided core.

iii. The amount of nitrogen which is required for building up the concentration profile in the ferrite matrix of the nitrided zone is negligible in comparison to the amount of nitrogen which is consumed at the reaction interface.

iv. Diffusion of Me can be neglected and is not nitriding-rate determining.

v. Local equilibrium prevails at the nitriding medium / specimen interface, so that the surface concentration $c_{N_\alpha}^S$ is equal to the lattice solubility of nitrogen, as given by the chemical potential of nitrogen in the nitriding atmosphere.

If these conditions are satisfied, it follows for the nitriding depth, X, at constant temperature:

$$X^2 = \left(\frac{2 \cdot c_{N_\alpha}^S \cdot D_N}{n \cdot c_{Me}} \right) \cdot t \tag{31}$$

where c_{Me} is the atomic concentration of substitutional solute Me originally dissolved, D_N is the diffusivity of nitrogen and *n* is the atomic ratio *N/Me* in the nitride phase formed by nitriding.

This model has been often used to predict the case depth of the nitrided zone [12-15]. However, a sharp interface between nitrided and unnitrided zone, as required by the model, does not occur in reality [12, 13]. Further, a major simplification of reality in the model is that the solubility of nitrogen in the ferrite matrix is taken as that pertaining to unstrained, pure α-Fe: the presence of excess nitrogen dissolved in the α-Fe matrix is not accounted for (see section 7.1). These shortcomings of the simple model have been overcome in the numerical model proposed in Ref. [13].

Henry's law holds for the nitrogen dissolved in α-Fe and hence it follows from Eq. (9) that $c_{N_\alpha}^S \sim a_N^S \sim r_N$. Then, considering the highly simplified model yielding Eq. (31), it can be suggested that the nitriding depth must be approximately proportional to $(r_n)^{1/2}$. However, at low nitriding potentials, nitriding of iron-based alloys could be lower than the expected [12]. At low nitriding potential, the value of $c_{N_\alpha}^S$ can be slightly lower than equilibrium solubility of nitrogen in the ferrite [12, 4]. This can be explained as follows. At relatively low nitriding potential, a significantly large finite period of time is necessary to establish local equilibrium of the gas atmosphere with the solid substrate. This effect has been observed for the nitriding of pure iron and is due to the finite rate of dissociation of NH_3 [16, 17]. The effect can be stronger for iron-based alloys at low nitriding potential, because in the presence of Me much more nitrogen has to be taken up before saturation at the surface can be attained. Apparently, for the iron-based alloys nitrided at low nitriding potentials, lower thickness (than the expected) could develop if the nitriding time applied is too short to achieve saturation at the surface.

Case depth can be measured by using various methods, such as microstructural investigation of the cross-section of the surface alloyed specimens (by using optical microscope and scanning electron microscope (SEM)), microhardness-depth profiling and elemental concentration-depth profiling (by using electron probe microanalysis (EPMA)) etc. If case depths are very thin, then specimen can be cut as shown in the Figure 5 with some angle, θ, and then such obtained cross-section will be investigated by using the methods mentioned above.

depth << L (depending upon value of θ)

depth = L * sin(θ)
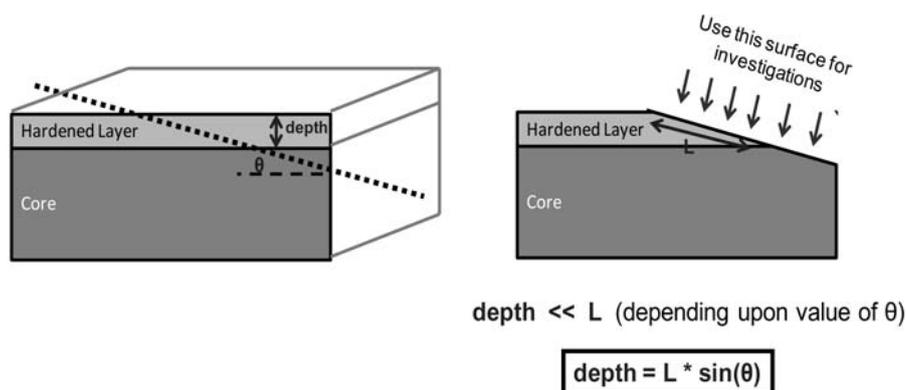
Figure 5. Scheme for determining case depth of thin layer.

Improvement in mechanical properties due to surface alloying

It is well know that the mechanical properties, like hardness, wear-resistance and fatigue strength, of the specimen are improved due to the surface alloying. These improvements in the properties are directly related the formation of new phases (e.g. compounds of alloying elements) and development of residual stresses/strains in the surface layer during surface-alloying treatment. Residual stress/strains are of two types: (i) macro- stress/strain, and (ii) micro- stress/strain.

The development of macro- stress/strain during surface alloying is shown in Figure 6. Consider the specimen in contact with the nitriding or carburizing media. In figure, N and C represent nitrogen and carbon, respectively. When the high chemical potential of N/C in the atmosphere is greater than the chemical potential of N/C in the specimen, N/C will dissolved in the surface until equilibrium is established at the surface. Introduction of the external species, here N/C, into the surface causes the expansion of the surface layer (Figure 6 (1) and (2)). However, the expansion is resisted by the non-treated core (Figure 6 (3)). Therefore, compressive residual stress is developed in the surface and tensile stress in the immediate region of the core. The magnitude of the residual stress changes with change in the concentration of surface alloying element (Figure 7). At a given process parameter of surface alloying treatment, surface has high concentration of the element and it decreases with increase in the depth. Such concentration-depth profile leads to the maximum compressive stress at the surface and stress decreases with depth. Such behavior is observed in the low temperature carburized austenitic stainless steel [21]. The presence of macro-stress/strain can be confirmed by using x-ray measurements. Shift in the x-ray diffraction peak position in intensity versus 2θ plot occurs if macro- stress/strain is present at the surface (Figure 8).
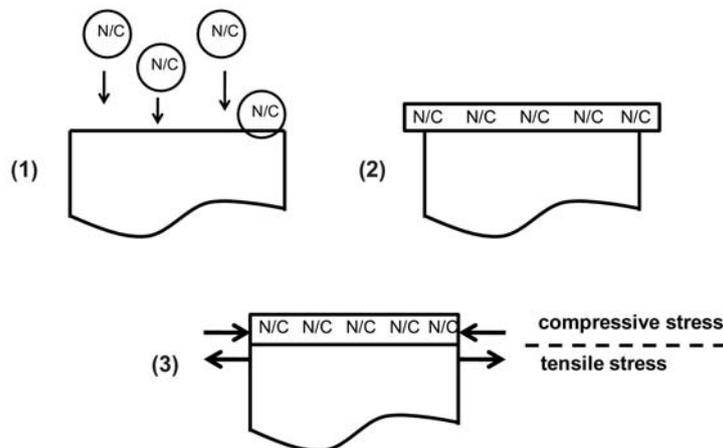
Figure 6. Schematic presentation of the development of residual macro- stress/strain at the surface of specimen during surface alloying. N and C represent nitrogen and carbon, respectively.
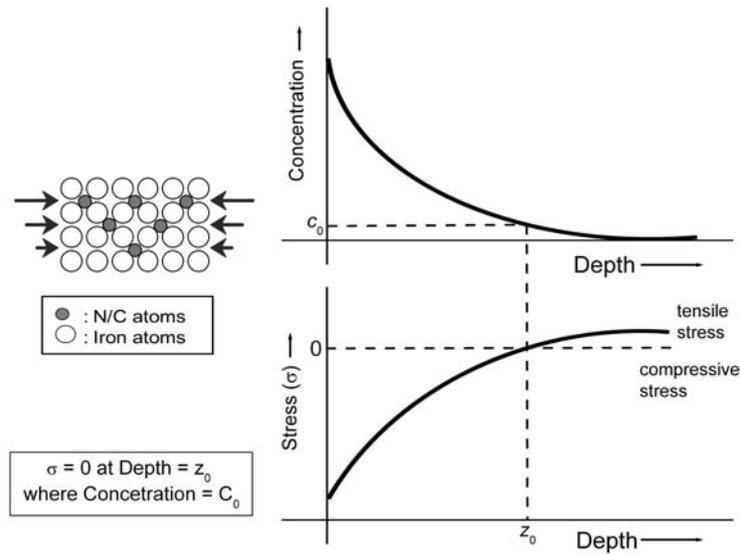
Figure 7. Schematic presentation of the change in the residual macro- stress/strain with concentration of surface alloying elements.
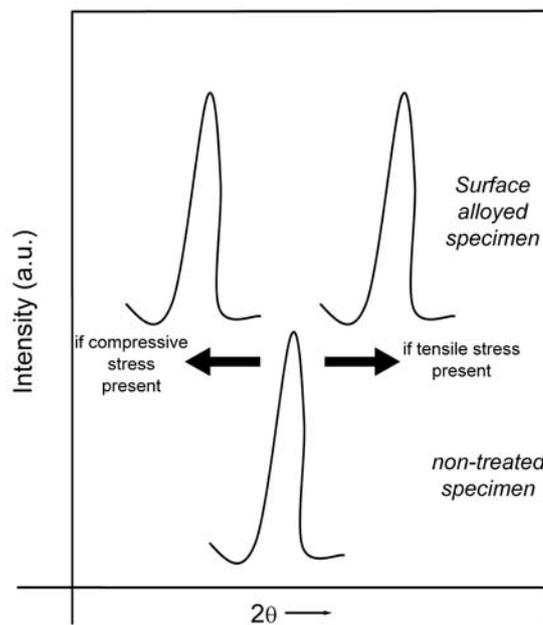
Figure 8. Schematic x-ray diffraction peak recorded from the surface of non-treated specimen and surface alloyed specimen. Peak shifts to leftwards if compressive stress/strain is present and it shifts rightward if tensile stress is present.

In many situation, the surface alloying of ferrous alloys leads to the formation of new phases, like nitride- or carbide- precipitates. If the lattice parameter of new phase is different than the matrix, misfit-strain field (micro- stress/strain) establishes surrounding the precipitates (Figure 9). The localized change in the lattice parameter of the matrix surrounding the precipitates, leads to the broadening of x-ray diffraction peak of the matrix phase (Figure 10). The hardness of the metals can be defined as the resistance to plastic deformation. This resistance is directly related to the resistance to the motion of dislocations. Presence of the hard precipitates in the soft matrix offers resistance to the motion of dislocation and hence, hardness increases. The presence of strain field surrounding the precipitates further increases the resistance to the motion of dislocation. If coarsening of the precipitates occurs, coherent interface between precipitate and matrix is replaced by the incoherent interface. In such situation, strain field is relaxed and dislocations are formed along the interface.

Both macro- and micro- stress are responsible for the improvement in fatigue resistance because compressive stress at the surface delays the crack initiation while the latter helps in delaying the crack propagation. However, the improvement in hardness (and hence, wear resistance) is related to the formation of new hard phases (like precipitates) and micro- stress associated with them. If the precipitate and micro- stress formation do not occur, the improvement in wear resistance will not be significant; for example, shot-peening improves the fatigue resistance, but not the wear resistance. Table 1 summarizes the properties and the cause for their improvements in surface alloyed specimens.

Table 1. Summary of the properties and the cause for their improvements in surface alloyed specimens.

Mechanical property	Reason for the improvement in property
Fatigue resistance	(Macro-stress) + (Micro-stress)
Hardness	(Micro-stress) + (Mechanical Property of new phases formed) + (Dislocation locking by interstitial atoms) + (In case of sever plastic deformation, interaction between dislocations)
Wear resistance	Hardness
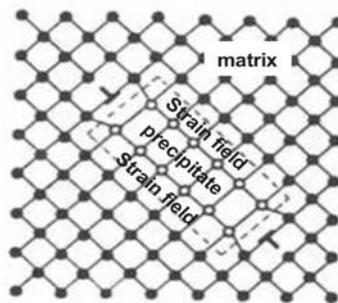
Figure 9. Schematic presentation of formation of precipitate in the matrix. Here, lattice parameter of the precipitate is different than the lattice parameter of matrix phase which leads to the formation of strain-field around precipitate.
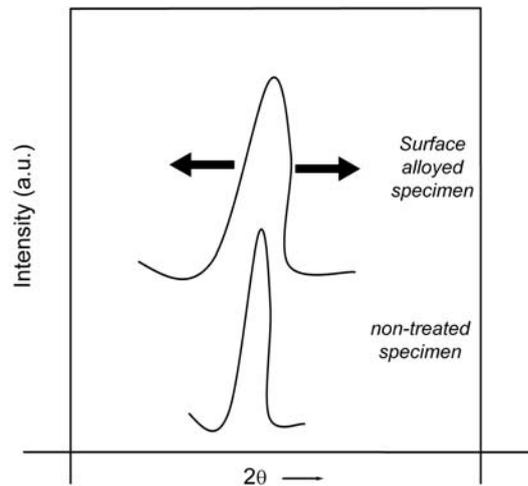
Figure 10. Schematic x-ray diffraction peak recorded from the surface of non-treated specimen and surface alloyed specimen. Peak broadening occurs due to the presence of micro- stress/strain in the surface alloyed specimen.

Some of the exciting researches in nitriding and carburizing

Nitriding of Fe-Me alloys and occurrence of excess nitrogen

During nitriding, if the iron matrix (substrate) contains alloying elements with a relatively high affinity for nitrogen, like Ti, V, Cr, Mn and Al, nitride precipitates can develop (in the "diffusion zone"), which leads to a pronounced increase of the hardness. The increase in hardness or fatigue resistance depends on the chemical composition of the precipitates, their coherency with the matrix, size and morphology.

If a Fe-Me (Me= Ti, V, Cr etc) alloy is nitrided such that no iron nitrides can be formed at the surface (i.e. the nitriding potential is sufficiently low), only a diffusion zone containing MeN_n precipitates develops ("internal nitriding") [12, 13]. The nitrided zone is composed of nitride precipitates and surrounding α-Fe (ferrite) matrix containing nitrogen at octahedral interstitial sites. For MeN_n precipitate in α-Fe the nitride platelets have the orientation $(001)_{\alpha\text{-Fe}}$ // $(001)_{MeNn}$, which is compatible with the Bain orientation relationship [18].

Nitrided Fe-Me alloys have a considerable capacity for the uptake of so-called excess nitrogen, i.e. more nitrogen than necessary for (i) precipitation of all alloying element as nitride, $[N]_{MeN_n}$, and (ii) equilibrium saturation of the ferrite matrix, $[N]_{\alpha}^{0}$. The total amount of excess nitrogen can be divided into two types: mobile and immobile excess nitrogen.

A significant part of the excess nitrogen in nitrided binary iron-based alloys is adsorbed at the nitride/matrix interfaces, $[N]_{interface}$. A MeN_n precipitate with excess nitrogen adsorbed at the interface with the matrix can be regarded as a MeN_X compound, i.e. (X-n) nitrogen atoms per MeN_X molecule are bonded / adsorbed to the coherent faces of the particle / platelet. The amount of nitrogen at the precipitate /

matrix interface is called immobile excess nitrogen as it does not take part in the kinetic process.

The coherent MeN_n precipitates induce strain fields in the surrounding ferrite matrix and thereby influence the nitrogen solubility of the ferrite matrix [19]. A MeN_n precipitate developing in the ferrite matrix experiences a positive volume misfit. Then, supposing fully elastic accommodation, the treatment by Eshelby [20] for a finite matrix shows that a positive dilation of the matrix occurs. The matrix lattice dilation generated by the misfitting nitrides, induced by the hydrostatic component of the image-stress field of finite bodies, provides a geometrical understanding for the occurrence of enhanced solubility of nitrogen. This dilation is not a direct function of temperature. The actually occurring, temperature dependent amount of excess nitrogen (at strain fields: $[N]_{strain}$) can then be estimated applying the thermodynamics of (hydrostatically) stressed solids [19]. The amount of nitrogen at strain fields is called mobile excess nitrogen as it takes part in the diffusion (kinetic) process.

Total nitrogen uptake by nitrided Fe-Me system can be subdivided (for easy understanding) as shown in Figure 11. Nitrogen absorption isotherms can be a useful tool to understand the various kinds of differently (chemically) bonded nitrogen (see Ref. [21] for details).

mobile nitrogen

immobile nitrogen

$$c_N = [N]_\alpha^0 + [N]_{MN_n} + [N]_{interface} + [N]_{dislocation} + [N]_{strain}$$

"normal" N content   total "excess nitrogen"

mobile excess nitrogen:
$[N]_{strain}$

immobile excess nitrogen:
$[N]_{dislocation}$ **and** $[N]_{interface}$
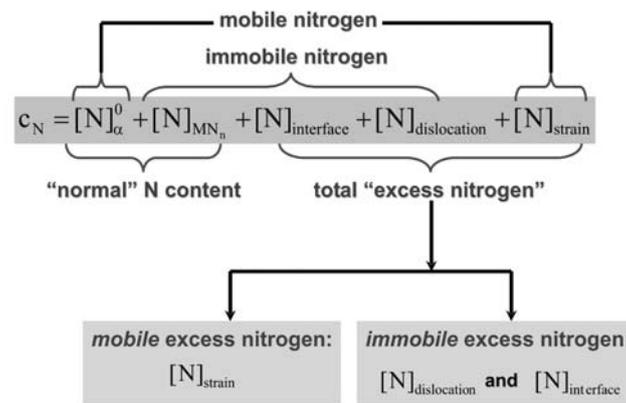
Figure 11. Flow chart indicating subdivision of nitrogen uptake in nitrided Fe-Me alloys. The amount of $[N]_{dislocation}$ can be neglected in recrystallized samples due to the relatively low dislocation densities.

Diffusion zone of the nitrided Fe-Cr and Fe-V alloys consists of nitrides of nitride-forming alloying elements plus ferrite matrix containing dissolve nitrogen (see Figure 12). Interestingly, these alloys show *two types* of the nitride precipitation morphologies: (i) fine precipitates with coherent or partly coherent interfaces with the iron matrix, and (ii) discontinuous coarsened precipitates where the fine nitride particles are replaced by a lamella-like morphology consisting of nitride and ferrite lamellae [13, 22]. The type of precipitation morphology is very much dependent on the concentration of the alloying elements. Alloys with high concentration of the alloying elements (above ~ 2 wt.%) show the discontinuous coarsened precipitation morphology [22, 23]. The coarsening of the nitride precipitates occurs possibly due to the reduction of Gibbs

energy as a result of relaxation of the internal long-range stress fields and of reduction of the precipitate/matrix interfacial area. This coarsening can of course in general be realized by continuous growth of the (largest) precipitates ("Ostwald ripening"), but, for the Fe-Cr and Fe-V alloys with high concentration of the alloying elements, it can in particular occur by a discontinuous coarsening of the former fine coherent or semi-coherent precipitates, involving growth of α-Fe and nitride lamellae from nucleation sites as surfaces and grain boundaries [22]. The driving force for the discontinuous coarsening reaction will be the larger the larger the amount of nitride precipitates. Therefore, the concentration of alloying elements play an important role in deciding the nitride-precipitation morphology in the nitrided alloys. Discontinuous coarsening causes decrease in the hardness and the nitrogen-uptake capacity due to the relaxation of stress field surrounding the precipitates.
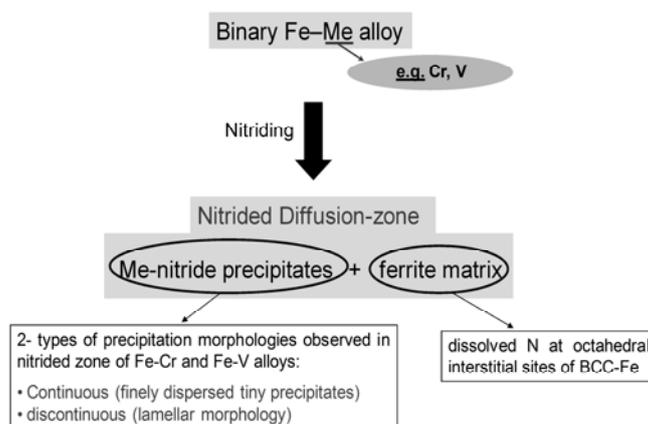
Figure 12. Flow chart summarizing the constituents of diffusion zone of nitrided Fe-Cr and Fe-V alloys.

Low temperature carburizing

One of the interesting developments in surface alloying is the low temperature carburizing developed by the researchers in the USA [24, 25]. Highlights of some the results obtained by them are as follows.

Conventional gas carburization of stainless steels is performed at up to 1010 °C. Hardness values can be increased from ~200 HV to between 700 and 750 HV. The improvement in hardness is due to the formation of chromium-carbides in the microstructures. However, the formation of chromium-carbides affects corrosion property because chromium is no longer available for the formation of passive chromium-oxide film. The precipitation of chromium carbides requires diffusion of substitutional elements (here, chromium). Substitutional element diffusion can be many orders of magnitude slower than interstitial diffusion of carbon. Therefore, a processing temperature window exists where significant carburization depths can be achieved while kinetically suppressing carbide formation. Low temperature carburization of 316 stainless steel at 470 °C had produced carbon concentration more than 10 at.% while maintaining single phase austenite. As a result of this, hardness of 1200 HV, surface compressive residual stress values of ~2.1 GPa and enhanced corrosion resistance were observed.

Conclusions

The fatigue, tribological and/or anti-corrosion properties of less expensive grades of alloys are possible to improve by using the surface alloying treatments such as carburizing, nitriding and chromizing. The mechanism of the surface alloying involves the following three important steps: absorption of diffusing species at specimen surface, inward diffusion of the absorbed species, and formation of compounds in the surface-treated region.

Composition of the surface, formation of the phases, and case-depth depend strongly on the temperature and chemical-potential of the species (here, nitrogen, carbon and chromium) in atmosphere surrounding the specimen.

Improvements in the mechanical properties of the surface due to the surface alloying are directly related to the formation of new phases (e.g. compounds of alloying elements) and the development of residual macro-/micro- stresses/strains in the surface layer. Due to the surface alloying, compressive residual macro-stress is developed in the surface and tensile stress in the immediate region of the core. The magnitude of the residual stress changes with change in the concentration of surface alloying elements. Both macro- and micro- stress are responsible for the improvement in fatigue resistance. However, the improvement in hardness (and hence, wear resistance) is related to the formation of new hard phases (like precipitates) and micro-stress associated with them. If the precipitates and micro-stress formation do not occur, the improvement in wear resistance will not be significant.

Few of the interesting results about nitriding of binary Fe-Cr and Fe-V are the presence of "excess nitrogen" and two-types of nitride-precipitation morphologies in the nitrided region. In case of carburizing, the concept of low temperature carburizing of stainless steels, which was developed by the researchers in the USA, is innovative. Such surface treatment on austenitic stainless steel resulted in the surface hardness of 1200 HV, surface compressive residual stress values of ~2.1 GPa and enhanced corrosion resistance.

References

[1]   M.A.J. Somers, Heat Treat. Met. 27 (2000) 92.
[2]   H.J. Grabke, Arch Eisenhüttenw 46 (1975) 75.
[3]   E.J. Mittemeijer, J.T. Slycke, Surface Engineering 12 (1996) 152.
[4]   E.J. Mittemeijer, M.A.J. Somers, Surface Engineering 13 (1997) 483.
[5]   B.J. Kooj, PhD Thesis, Delft University of Technology, The Netherlands, 1995.
[6]   D.A. Porter, K.E. Easterling, Phase Transformations in Metals and Alloys, Van Nostrand Reinhold Co. Ltd., UK, 1981.
[7]   H.A. Wriedt, N.A. Gokcen, R.H. Nafziger, Bulletin of Alloy Phase Diagrams 8 (1987) 355.
[8]   H.J. Grabke, Ber. Bunsengesell. Physic. Chem. 72 (1968) 533.
[9]   W.D. Callister, Materials Science and Engineering, John Wiley & Sons Inc., USA, 2007.
[10]   J.D. Fast, M.B. Verrijp, Journal of the Iron and Steel Institute 176 (1954) 24.
[11]   J.L. Meijering, Advances in Material Research, Vol. 5, Wiley Interscience New York, 1971.
[12]   S.S. Hosmani, R.E. Schacherl, E.J. Mittemeijer, Mater. Sci. Technol. 21 (2005) 113. (doi: 10.1179/174328405X16289)

[13]   R.E. Schacherl, P.C.J. Graat, E.J. Mittemeijer, Met. & Mat. Trans. 35A (2004) 3387.

[14]   E.J. Mittemeijer, A.B.P. Vogels, van der P.J. Schaaf, J. Mater. Sci. 12 (1980) 3129.

[15]   P.M. Hekker, H.C.F. Rozendaal, E.J. Mittemeijer, J. Mater. Sci. 20 (1985) 718.

[16]   H.C.F. Rozendaal, E.J. Mittemeijer, P.F. Colijn, van der P.J. Schaaf, Metall. Trans. 14A (1983) 395.

[17]   P.B. Friehling, F.W. Poulsen, M.A.J. Somers, Zeitschrift fuer Metallkunde 92 (2001) 589.

[18]   T.C. Bor, A.T.W. Kempen, F.D. Tichelaar, E.J. Mittemeijer, van der E. Giessen, Phil Mag 82A (2002) 971.

[19]   M.A.J. Somers, R.M. Lankreijer, E.J. Mittemeijer, Phil. Mag. 59A (1989) 353.

[20]   J.D. Eshelby, Solid State Physics 3 (1956) 79.

[21]   S.S. Hosmani, R.E. Schacherl, E.J. Mittemeijer, Acta Mater. 54 (2006) 2783. (DOI: 10.1016/j.actamat.2006.02.017)

[22]   S.S. Hosmani, R.E. Schacherl, E.J. Mittemeijer, Acta Mater. 53 (2005) 2069. (DOI: 10.1016/j.actamat.2005.01.019)

[23]   S.S. Hosmani, R.E. Schacherl, E.J. Mittemeijer, J. Mater. Sci. 43 (2008) 2618-2624. (DOI: 10.1007/s10853-008-2473-9)

[24]   G.M. Michal, F. Ernst, H. Kahn, Y. Cao, F. Oba, N. Agarwal, A.H. Heuer, Acta Mater. 54 (2006) 1597.

[25]   Y. Cao, F. Ernst, G.M. Michal, Acta Mater. 51 (2003) 4171.